NASA TECHNICAL TRANSLATION NASA TT F- 14,771

MIRROR OPTICS OF X-RAY TELESCOPES AND A DESCRIPTION OF A PROGRAM FOR DESIGN OF AN OBJECTIVE

I. L. Beygman, L. A. Vaynshteyn, Yu. P. Voynov and V. P. Shevel'ko

(NASA-TT-F-14771) MIRROR OPTICS OF X-RAY TELESCOPES AND A DESCRIPTION OF A PROGRAM FOR DESIGN OF AN OBJECTIVE (Kanner (Leo) Associates) 44 p HC $5.25 CSCL 20F G3/14

N74-20013

Unclas 29048

Translation of
"Zerkal'naya Optika Rentgenovskikh Teleskopov i Opisaniye Programmy Dlya Rascheta Obbektive," Academy of Sciences USSR, P. N. Lebedev Physics Institute, Preprint No 112, 1973., 61 pages

NATIONAL AERONAUTICS AND SPACE ADMINISTRATION
WASHINGTON, D. C. 20546 OCTOBER 1973

STANDARD TITLE PAGE

1. Report No. NASA TT F-14,771	2. Government Accession No.	3. Recipient's Catalog No.
4. Title and Subtitle MIRROR OPTICS OF X-RAY TELESCOPES AND A DESCRIPTION OF A PROGRAM FOR DESIGN OF AN OBJECTIVE		5. Report Date Oct 73 6. Performing Organization Code
7. Author(s) I. L. Beygman, L. A. Vaynshteyn, Yu. P. Voynov and V. P. Shevel'ko		8. Performing Organization Report No. 10. Work Unit No.
9. Performing Organization Name and Address Leo Kanner Associates P. O. Box 5187 Redwood City, California		11. Contract or Grant No. NASw-2481 13. Type of Report and Period Covered Translation
12. Sponsoring Agency Name and Address NASA,		14. Sponsoring Agency Code

15. Supplementary Notes Translation of "Zerkal'naya Optika Rentgenovskikh Teleskopov i Opisaniye Programmy Dlya Rascheta Obbektiva," Academy of Sciences USSR, P. N. Lebedev Physics Institute, Preprint No 112, 1973, 61 pages

16. Abstract

17. Key Words (Selected by Author(s))	18. Distribution Statement
	Unclassified. Unlimited.

19. Security Classif. (of this report)	20. Security Classif. (of this page)	21. No. of Pages	22. Price
None	None	44	5.25

NASA-HQ

MIRROR OPTICS OF X-RAY TELESCOPES AND A DESCRIPTION OF A PROGRAM FOR DESIGN OF AN OBJECTIVE

I. L. Beygman, L. A. Vaynshteyn, Yu. P. Voynov and V. P. Shevel'ko

Chapter 1. Mirror Systems for X-Ray Telescopes /3*

§1.1. Introduction

As we know, the study of the soft x-ray radiation of astrophysical objects by means of large-area proportional flow counters involve significant technical difficulties. However, in this area of the spectrum (softer than 1 KeV), mirror x-ray optics can be used. The use of mirror x-ray telescopes can be expediently studied in two aspects. On the one hand, mirror optics allow a comparatively large collecting area to be used with small detector dimensions, significantly decreasing the technical difficulties and increasing the signal/noise ratio; on the other hand, mirror objectives make it possible in principle to produce images similar to those yielded by telescopes in the ordinary visible range of the spectrum.

The first development and use of a device with mirror collecting optics (a parabolic mirror) for studies in the soft x-ray area of the spectrum was described in [1, 2]. A device of similar type, designed to be carried by a satellite, is described in [3].

X-ray mirror systems, producing an image in the focal plane, /4 have been the subject of a large number of works. H. Wolter [4, 5] showed that one necessary condition for production of an image is an even number of reflections. Detailed analysis of systems of confocal paraboloid and hyperboloid reflectors and an extensive bibliography can be found in review [6] and article [7]. Systems of this type were used to produce x-ray photographs of solar flares with resolutions of about 2 seconds [8]. A system with crossed parabolic mirrors is described and studied in [9].

The purpose of the present work is investigation of the collecting systems (cone, parabaloid) and objectives (combination of paraboloid and hyperboloid) from the standpoint of the production of the greatest effective area with fixed dimensions of the system. Since an x-ray mirror system has a tubular shape,

*Numbers in the margin indicate pagination in the foreign text.

with the diameter significantly less than the length, the basic limiting dimension is considered to be the length, i.e., the focal length of the system. For the combination of a paraboloid with a hyperboloid, we also note the distribution of intensity in the focal plane as a function of the angle of the parallel bundle of rays with the axis of the system. This distribution allows us to make a judgment concerning aberrations and the resolving power of the lenses.

The small diameter of the entry window of the detector used with mirror systems makes it possible to use semiconductor detectors and channeltrons as well as gas counters. The prospects for the use of these detectors are studied in §1.7.

§1.2. Reflection Factor /5

Modern mirror x-ray optics are based on the phenomenon of total "external" reflection. X-rays can be effectively reflected from surfaces, i.e., the index of refraction of a substance for x-rays may be less than 1. The index of refraction can be written as:

$$n = 1 - \delta - i\beta \qquad (1.1)$$

For the x-ray area of the spectrum, upon transition from air to the substance, the quantities δ and β are positive and low in absolute value. Since the real portionof the index of refraction is less than 1, there is an angle of total "external" reflection, defined by the condition

$$\cos \phi_0 = 1 - \delta, \qquad (1.2)$$

where ϕ_0 is the angle between the ray and the reflecting surface.

For small δ, condition (1.2) can be rewritten as:

$$\phi_0 = \sqrt{2\delta} \qquad (1.2a)$$

If the imaginary portion (β) of the index of refraction, responsible for absorption, were equal to 0, then the reflection factor (κ) would be equal to 1 for angles less than ϕ_0. The presence of absorption results in a significant reduction in reflection for angles less than ϕ_0.

The reflection factor, considering absorption, is given by the Fresnel formulas. At low angles it is: /6

$$\kappa(\varphi) = \frac{(\varphi - \theta_1)^2 + \theta_2^2}{(\varphi + \theta_1)^2 + \theta_2^2}$$

$$\theta_1 = \frac{1}{\sqrt{2}}\left[\sqrt{(\varphi^2 - 2\delta)^2 + 4\beta^2} + (\varphi^2 - 2\delta)\right]^{1/2}$$

$$\theta_2 = \frac{1}{\sqrt{2}}\left[\sqrt{(\varphi^2 - 2\delta)^2 + 4\beta^2} - (\varphi^2 - 2\delta)\right]^{1/2} \qquad (1.3)$$

For x-ray mirrors, there is particular interest in the use of strong coatings, for which the reflection factor is high at comparatively great slipping angles.

Systematic measurements of the reflection factor for various coatings as a function of the incident angle and wave length of incident x-ray radiation have been performed by the group of Lukirskiy (see [10, 11]). It follows from these works [10, 11] that the most promising materials for coating of x-ray mirrors are nickel and gold. Reflection factors for these elements are presented in Figures 1 and 2. Parameters δ and β, taken from [10], are presented in Table 1.

TABLE 1

Substance	λ, [Å]	$\frac{\beta}{\delta}$	$\delta \cdot 10^{+4}$	$\frac{\delta}{\lambda^2}$	$\beta \cdot 10^{+4}$
1	2	3	4	5	6
Ni	8.34	0.32± 0.03	5.91± 0.17	8.48	1.9± 0.2
	9.89	0.40± 0.04	8.00± 0.20	8.17	3.2± 0.3
	10.44	0.50± 0.05	8.70± 0.20	8.15	4.4± 0.4
	12.25	0.60± 0.06	8.85± 0.21	5.90	5.3± 0.5
	13.34	0.70± 0.07	10.20± 0.22	5.72	7.2± 0.7
	14.56	7.00± 0.70	1.37± 0.08	0.65	9.6± 1.0
	15.97	0.17± 0.02	12.30± 0.20	4.83	2.1± 0.2
	17.59	0.16± 0.02	17.50± 0.30	5.65	2.8± 0.3
	19.4	0.17± 0.02	21.70± 0.30	5.74	3.7± 0.4
	21.64	0.20± 0.02	30.50± 0.40	6.50	6.1± 0.6
	23.62	0.22± 0.02	33.30± 0.40	5.98	7.3± 0.7

/7

1	2	3	4	5	6
Ni	24.78	0.23± 0.02	39.40± 0.44	6.43	9.1± 0.9
	27.42	0.21± 0.02	47.30± 0.48	6.30	10.0± 1.0
	31.36	0.25± 0.03	60.00± 0.50	6.12	15.0± 1.5
Au	8.34	0.34± 0.03	9.15± 0.21	13.10	3.1± 0.3
	9.89	0.38± 0.04	11.50± 0.24	11.75	4.4± 0.4
	12.254	0.52± 0.05	18.00± 0.30	12.00	9.4± 0.9
	13.34	0.58± 0.06	21.20± 0.30	11.90	12.3± 1.2
	14.56	0.65± 0.07	24.10± 0.30	11.40	15.7± 1.6
	15.97	0.70± 0.07	26.60± 0.40	10.45	18.6± 1.9
	17.59	0.80± 0.08	29.20± 0.40	9.45	23.4± 2.3
	19.45	0.80± 0.08	33.50± 0.40	8.85	26.8± 2.7
	21.64	0.82± 0.08	34.80± 0.40	7.43	28.5± 2.9
	23.62	1.00± 0.10	37.60± 0.40	6.75	37.6± 3.8
	24.78	1.40± 0.10	40.00± 0.40	6.50	56.0± 5.6
	27.42	1.50± 0.20	40.80± 0.50	5.44	61.0± 6.0
	31.36	1.30± 0.10	47.50± 0.50	4.85	61.5± 6.2

/8

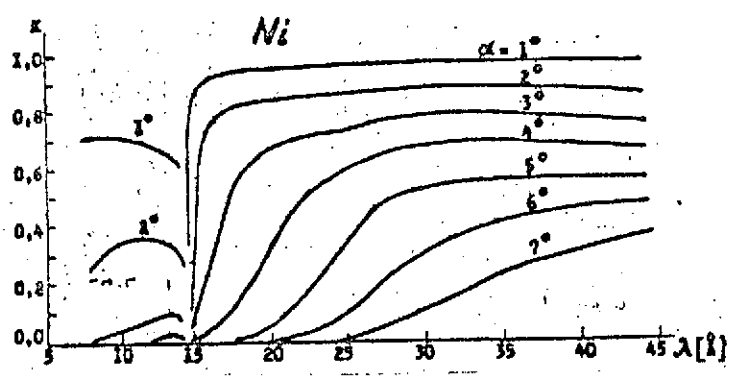

Figure 1. Reflection Factor of Nickel

/9

The values of δ and β for nickel at 44.4 A wavelength, used in our subsequent calculations, were determined by computer on the basis of the known reflection factor (Figure 1) for three slipping angles: 4°, 7° and 8°. The following quantities were produced: $\delta = 10^{-2}$; $\beta = 35 \cdot 10^{-4}$.

It should be noted that the reflection factor in the x-ray area depends strongly on the quality and technology of manufacture of surfaces and requires special testing.

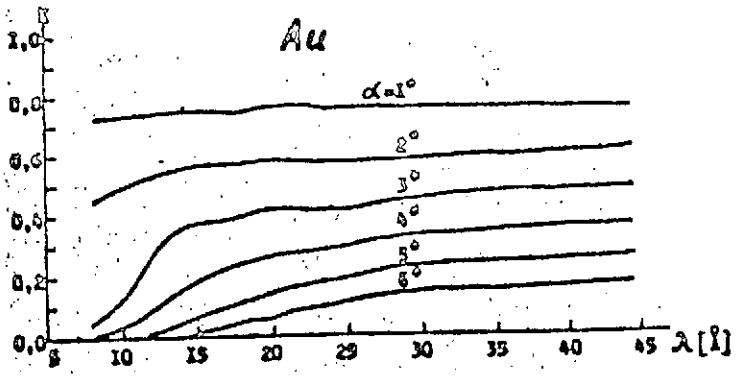

Figure 2. Reflection Factor of Gold

§1.3. Collecting Mirrors

1.3.1. Cone

The simplest collecting mirror for x-ray astronomy is the cone (Figure 3). It allows the radiation flux density parallel to the main optical axis to be increased by

$$\frac{8 \cdot R_0 \cdot \cos 2\varphi}{d} \cdot k(\varphi) \quad \text{times}, \qquad (1.4)$$

where d is the diameter of the counter window,

$k(\phi)$ is the reflection factor for a given glancing angle ϕ of the incident beam,

R_0 is the mean diameter of the cone.

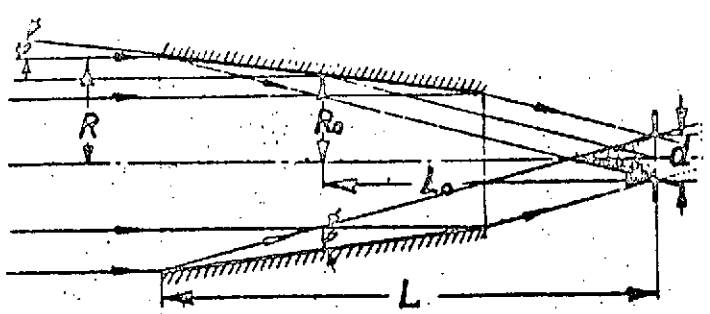

Figure 3. A Conical Mirror

It is easy to show that in this case, the ratio of the signal level to the level of noise fluctuations (signal/noise$^{1/2}$) is independent of detector window diameter. /10 /11

In addition to its main task, that of collecting the flux, the cone acts simultaneously as a collimator with an angle of view (at half width) $\Delta\phi \approx \pm 0.4\ d/L_0$, where L_0 is the distance from the counter window to the center of the working portion of the cone.

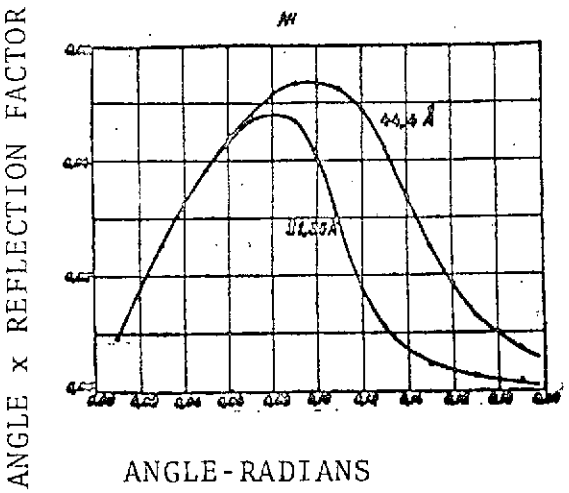

Figure 4. Effective Area for a Nickel Cone as a Function of Glancing Angle

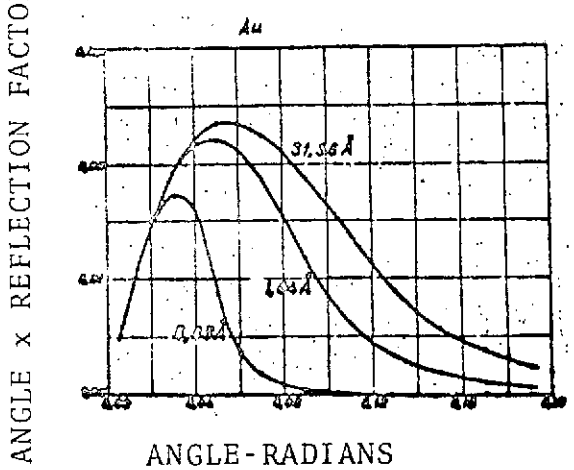

Figure 5. Effective Area for a Gold Cone as a Function of Glancing Angle

The effective area of an x-ray telescope with a collecting cone is:

$$S_{ef} = 2\pi d^2 \cdot \cos 2\phi \cdot \cdot \cos \phi \, (2(L/d) \sin \phi - \cos \phi) \cdot k(\phi) \qquad (1.5)$$

where L is the distance from the window of the detector to the entry aperture.

The minimum angle (ϕ_m) for which the parallel bundle of rays, after reflection, still completely fills the window of the detector, is determined by the condition:

$$\phi_m \cong d/L \qquad (1.6)$$

Generally, $\phi > \phi_m$. In this case:

$$S_{ef} = 4\pi Ld \cdot [\phi \cdot k(\phi)] \qquad (1.7)$$

The optimal dimensions of the cone (R) for a fixed length (L), detector diameter (d) and known dependence of reflection factor $k = k(\phi)$ on slipping angle (see formula 1.3) for a given wavelength are determined from the condition of maximum effective area. The function $\phi \cdot k(\phi)$ for Ni (λ = 44.4 and 31.36 A) and Au (λ = 9.89; 21.64 and 31.36 A) is presented in Figures 4 and 5.

1.3.2 Paraboloid

A significantly greater gain in signal-to-noise ratio is achieved using parabolic mirrors. In this case, the useful /12

signal level is determined by the effective area of the collecting mirror, while the noise level is determined by the dimensions of the detector which, in principle, can be quite small.

A diagram of a parabolic mirror and symbols used are presented in Figure 6.

The equation for a paraboloid of rotation in these symbols is:

$$x^2 + y^2 = 2p \cdot (z_p - z), \tag{1.8}$$

where the z axis corresponds to the axis of symmetry and is the main optical axis. The parameter of the paraboloid (p) and distance from its point to the entry aperture of the mirror (z_p) are:

$$p = -L_p + \sqrt{L_p^2 + b^2},$$
$$z_p = \frac{b^2}{2p} \tag{1.9}$$

where b is the radius of the entry aperture of the paraboloid and L_p is the "focal" length of the paraboloid (distance from focal point to entry aperture).

The effective area of a parabolic mirror is:

$$S_{эф.} = 2\pi \int_0^b \rho \cdot \varkappa(\varphi) \cdot d\rho \tag{1.10}$$

where $\rho = \sqrt{x^2 + y^2}$, and the reflection factor is defined by formulas (1.3).

The dependence of effective area on parameters of the paraboloid (b, L_p and F) with a coating of nickel (for λ = 44.4, 31.36 and 21.64 A) and gold (for λ = 9.89, 21.64 and 31.36 A) is shown in Figures 7 and 8. /14

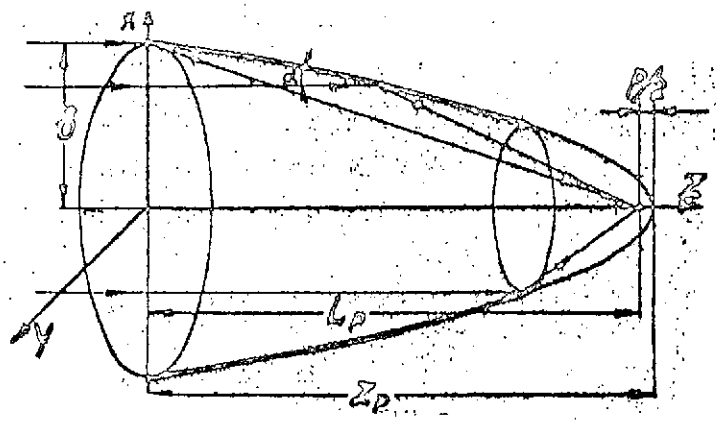

Figure 6. A Parabolic Mirror

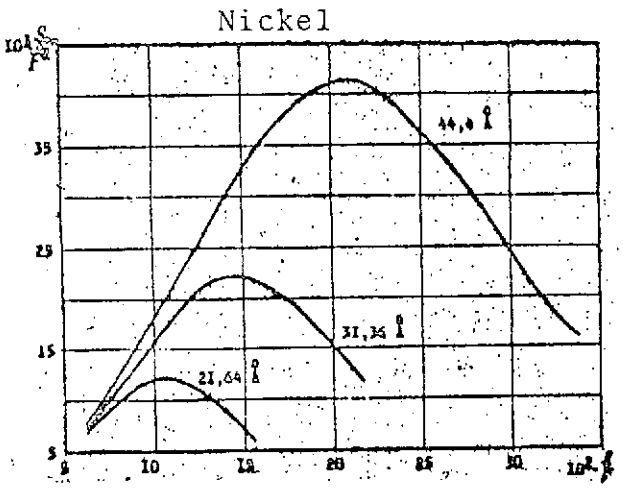

Figure 7. Effective Area as a Function of Entry Radius b and Focal Length F of a Paraboloid of Ni

We can see from Figures 7 and 8 that a paraboloid with a nickel coating can be expediently used for operation in the wavelength interval over 20 A. For the 10-20 A wavelength range, a gold coating produces a greater effective area. Calculations performed for coatings of aluminum show that it yields significantly lower effective area in these wavelength ranges. For the area $\lambda <$ < 10 A, it is not technically expedient to make mirror collecting optics of any materials known at the present time.

The dependence of effective area of a paraboloid on angle of the parallel bundle to the axis is determined by the dimensions of the detector. As an illustration, this dependence, determined by calculation, is presented in Figure 9 for a paraboloid with a nickel coating, wavelength 44 A and ratio b/F = 0.185. The field of vision $\Delta\alpha$ is approximately proportional to the dimensions of the detector $\Delta\alpha \sim d/F$. Detailed formulas for calculation of the paths of rays are presented in Chapter 2.

§1.4. Experimental Parameters of an X-Ray Telescope Parabolic Mirror for the 44-60 A Range

Parabolic mirrors of epoxy resin with aluminum coating and metal replicas with nickel coating were made for the soft x-ray spectral range of 44-60 A.

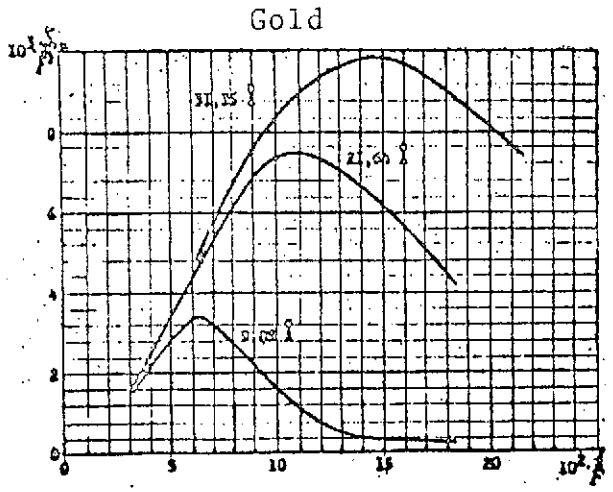

Figure 8. Effective Area as a Function of Engry Radius b and Focal Length F of a Paraboloid of Au

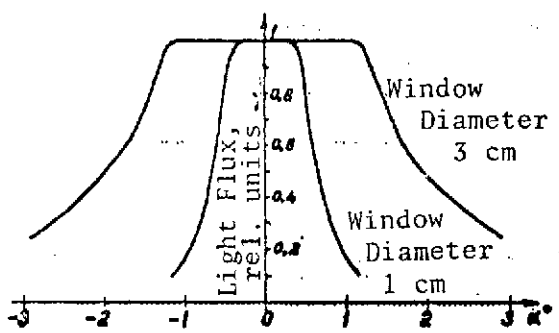

Figure 9. Calculated Dependence of S_{ef} on Angle of Parallel Bundle (λ = 44 A) with Axis. Nickel Paraboloid with F = = 65 cm, b = 12 cm

1.4.1. Epoxy Parabolic Mirror

A parabolic mirror of epoxy resin was produced by the method of spinning a solidifying solution (spinning speed n = 343 rpm), and measured b = 9.8 cm, F = 63 cm, parameter p = = 0.76.

The quality of the surface (agreement with formula $x^2 + y^2 = 2pz$) was tested in the fixible range with a collimator. The dimensions of the focal spot fell within the limits of divergence of the collimator (about 4.5 minutes). Thus, the variation of a perpendicular to the surface from its assigned angle is not over about 1 minute. /15

Aluminum was selected as a coating on the basis of the simplicity of the technology of vacuum spraying, and its comparatively high reflection factor in the 44 A range.

The angular dependence of reflection factor was measured with an x-ray crystal monochromator for a specimen cut from the finished epoxy mirror. the source of radiation used was an x-ray tube with a carbon anticathode. The working wavelength was the characteristic line of C_{k_d} (44.4 A) with a contrast of about 10, separated by a flat barium stearate crystal (lattice constant d = 50 A). The detector used was a proportional flow counter. The window was a film of cellulose nitrate varnish. Comparison of the experimentally measured reflection factor with the data from [10] in which aluminum sprayed onto polished glass was studied is illustrated by Figure 10. Test measurements of the reflection factor for aluminum on glass agreed with the results of [10]. /17

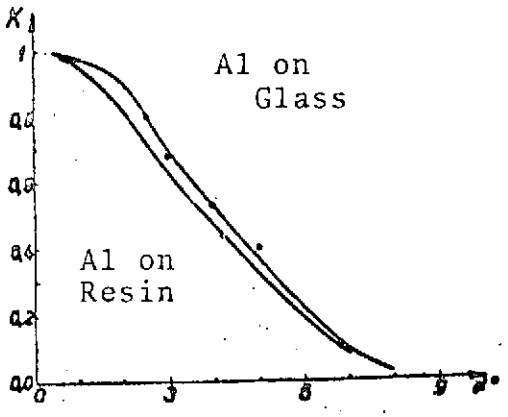

Figure 10. Reflection Factor for Aluminum, Sprayed onto Resin Paraboloid (Lower Curve); o, Measurements of Lukirskiy et al. (see II)

1.4.2. Metal Replicas

A metal parabolic mirror of nickel was made by electrolytic deposition on a matrix. A matrix with the optimal dimensions (F = 65 cm) for λ = 44 A, calculated by the method outlined above, was turned on a program-controlled lathe and polished by the usual methods. The first, working, layer deposited, was about 0.1 mm of nickel, followed by a layer of copper of the necessary thickness, generally 1.5-2 mm.

A mirror made by this method has a number of advantages over epoxy and glass mirrors. It is significantly lighter, requires no complex mount for its support, and is heat resistant. Furthermore, the coppying method allows a large number of mirrors to be produced from a single matrix, which is essential for satellite and rocket studies, when the instruments are lost. The focussing properties of the surface, which depend on the accuracy of manufacture of the paraboloid, were tested in the visible light range. To do this, a parallel bundle of rays (divergence about 10^{-3} rad) from a collimator was directed onto the mirror along its main optical axis. An iris diaphragm was placed at the focal point. The departing radiation was recorded by a photomultiplier. The result produced as to distribution of intensity of radiation at the focal point is represented graphically in Figure 11. The diameter of a spot including half the flux is 3 mm. This value is related primarily to errors in manufacture of the matrix. For an ideal parabola with this divergence the diameter should be about 0.7 mm.

We should note that the quality of manufacture achieved is hardly the greatest possible for programmed machine tools. Preliminary measurements show that replicas taken from a second matrix specimen yield a focussing spot about 1 mm in diameter. /19

The field of vision of the parabolic mirror was also determined in the visible area. The results of measurements presented in Figure 12 for detectors with inlet diameters of 10 mm and 30 mm are near the theoretical values (see Figure 9).

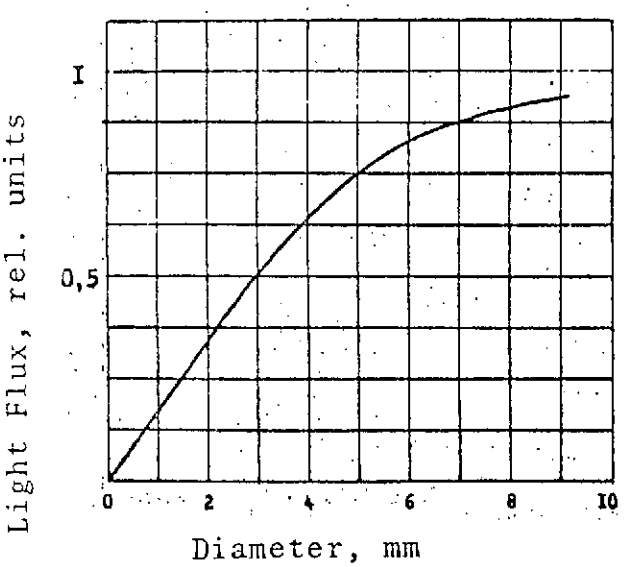

Figure 11. Experimental Dependence of Flux on Diameter of Detector Located in Focal Plane of Paraboloid

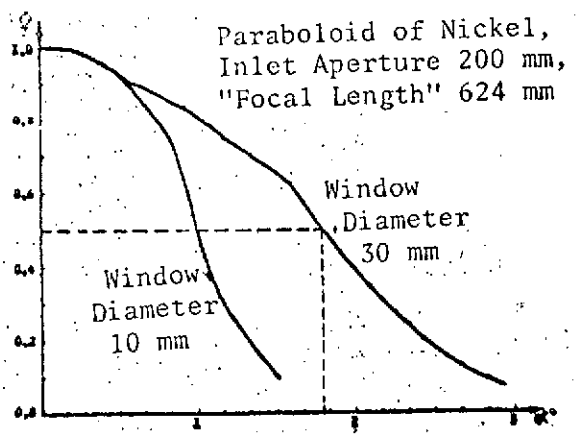

Figure 12. Light Flux Φ in Focal Plane as a Function of Angle of Parallel Bundle with Axis

The quality of polishing also determines the reflection factor in the x-ray area of the spectrum. The reflection factor was measured by the method described in 1.4.1. The results of experimental measurement are presented in Figure 13, together with data from [10]. /18

§1.5. Objectives /21

A paraboloid has great coma aberrations. Precise calculations show that for rays not on the axis, the angular dimensions of the aberrations exceed the angle of these rays to the axis. This prevents the production of an image by means of a paraboloid.

The Abbe sine condition must be fulfilled in an optical system forming an image without coma, i.e., the ratio $\sin\alpha/\sin\alpha'$ must be constant for all rays, α and α' being the angles between a given ray and the lines connecting a point in the plane of the object and the plane of the image.

Wolter [4, 5] showed that the sine condition is fulfilled with an even number of reflecting surfaces. In this sense, the most promising objective is one consisting of coaxial and confocal parabolic and hyperbolic reflectors. As we can see from Figure 14, the Abbe sign condition, which is not at all fulfilled

for a paraboloid, is approximately fulfilled for a paraboloid plus hyperboloid, since in the latter case α' decreases with decreasing α. Figure 15 shows a diagram and the symbols for such an objective.

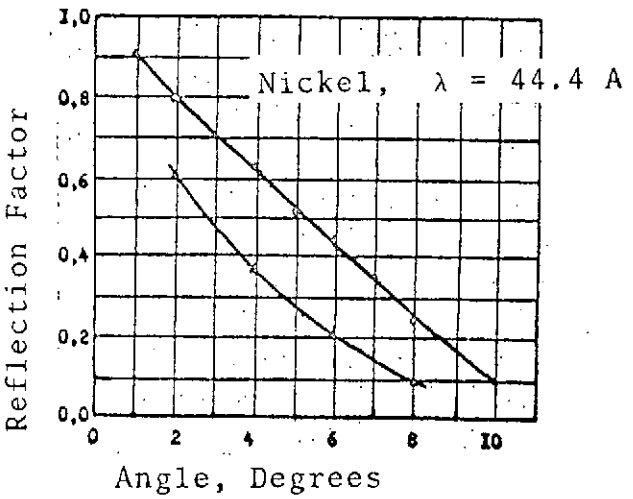

Figure 13. ▲ - Reflection Factor for Nickel Replica (λ = 44 A). ○ - Reflection Factor for Optically Polished Nickel Specimen (see [10]).

Single-Mirror System

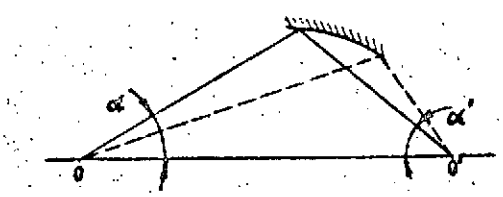

Dual-Mirror System

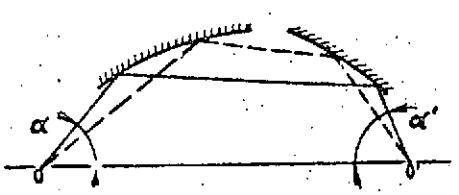

Figure 14. Abbe Sine Condition

The equation of the paraboloid in these symbols is:

$$x^2 + y^2 = 2p \cdot (z_p - z) \qquad (1.11)$$

and for the hyperboloid

$$-\frac{x^2 + y^2}{c^2} + \frac{(z - z_r)^2}{a^2} = 1 \qquad (1.12)$$

where p, c, a are the parameters of the paraboloid and hyperboloid,

z_p is the distance from the point of the paraboloid to the inlet aperture,

z_r is the distance from the center of the hyperboloid to the inlet aperture, /20 /22

The z axis coincides with the axis of symmetry of the system.

Detailed formulas for calculation of the paths of rays and parameters of the paraboloid and hyperboloid are presented in Chapter II (§2.2).

The effective areas, calculated with the reflection factor taken from [10, 11], for an objective with F = 65 cm with a nickel

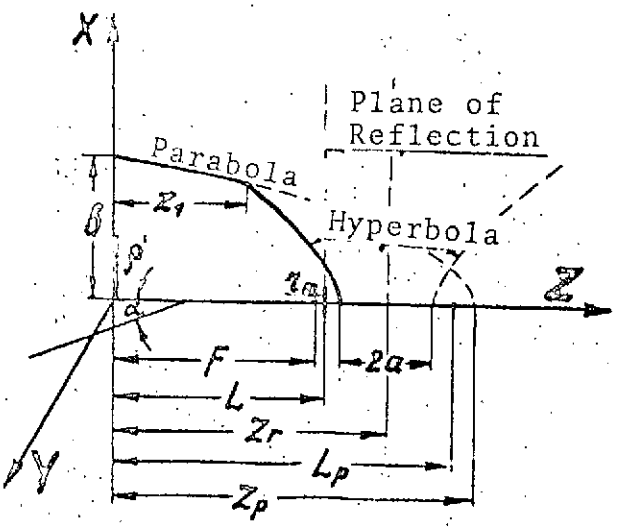

Figure 16. Paraboloid plus Hyperboloid Objective Plan

coating (λ = 21.6, 31.36 and 44.4 A) and a gold coating (λ = 9.89, 21.61 and 31.36 A) represented in Table 2.

The dimensions (b is the radius of the inlet aperture, L_p is the "focal" length of the parabola) are given in cm. The effective area is given in cm^2. The first row of the table (L_p = 65) corresponds to a single parabola. The numbers underlined correspond to the greatest effective areas for a paraboloid and for an objective consisting of a paraboloid and hyperboloid.

TABLE 2

Ni , λ =21,6 Å

L_p \ b	6	8	I0	I2	I4	I6
65	49,I	47,7	25,5	II,I	6,5	4,5
67	32,2	36,9	I8,4	5,8	2,4	I,2
69	30,3	39,9	22,8	7,I	2,8	I,4
7I	30,9	40,0	26,7	8,7	3,2	I,5
73	28,6	38,7	30,I	I0,5	3,7	I,9
75	26,I	40,2	34,6	I3,5	4,6	2,0
77	26,5	37,6	36,3	I6,I	5,3	2,2
79	23,8	34,3	36,I	20,I	6,7	2,7

Ni , λ = 31,36 Å

L_p \ b	4	6	8	I0	I2	I4
65	30,6	60,3	85,8	<u>92,6</u>	78,3	50,4
67	I8,4	36,0	53,6	64,I	57,8	33,I
69	I7,0	33,5	54,8	67,3	62,5	39,3
7I	I7,2	33,9	5I,5	64,9	65,0	45,2
73	I5,7	3I,2	47,8	6I,4	65,I	50,2
75	I4,2	28,3	48,6	63,2	<u>69,2</u>	57,4
77	I4,3	28,6	44,4	58,4	66,I	59,6
79	I2,7	25,5	39,8	52,9	69,I	65,5

/23

Ni, λ = 44,4 Å

L_p \ δ	I0	I2	I4	I6	I8	20
65	I44	I68	I73	I59	I30	94,8
67	85,9	II3	I22	II2	84,9	53,2
69	87,7	I09	I2I	II7	95,0	63,4
7I	82,I	I03	II7	II9	I03	76,7
73	75,9	95,8	III	I27	II5	86,7
75	77,I	90,0	II5	I23	II7	94,7
77	70,2	89,8	I06	II6	I26	I07
79	62,8	9I,5	I09	I2I	I23	II0

Au, λ = 9,89 Å

L_p \ δ	2	3	4	5	6	7
65	6,7	II,8	I4,2	I2,6	8,5	5,0
67	3,9	6,9	8,8	8,0	4,8	2,3
69	3,6	6,5	8,5	8,3	5,4	2,8
7I	3,7	6,6	8,8	9,0	6,4	3,3
73	3,4	6,I	8,3	8,9	6,8	3,7
75	3,I	5,6	7,7	8,5	7,I	4,I
77	3,I	5,7	7,9	9,0	7,9	4,9
79	2,8	5,I	7,2	8,3	7,7	5,2

Au, λ = 2I,6I Å

L_p \ δ	4	6	7	8	I0	I2
65	I9,9	29,6	3I,3	30,9	25,5	I8,3
67	I0,8	I5,2	I5,7	I5,0	I0,8	6,7
69	I0,I	I4,5	I6,7	I6,2	I2,3	7,3
7I	I0,3	I5,I	I6,I	I5,9	I2,6	7,9
73	9,6	I4,2	I5,2	I5,3	I2,7	8,2
75	8,7	I3,I	I4,2	I6,2	I3,9	9,4
77	8,9	I3,5	I4,8	I5,2	I3,5	9,6
79	8,0	I2,2	I3,5	I4,0	I2,8	I0,7

/24

Au, λ = 3I,36 Å

L_p \ δ	4	6	8	I0	I2	I4
65	20,6	33,2	40,4	4I,2	37,4	3I,5
67	II,I	I6,6	I8,7	I7,4	I5,I	I0,7
69	I0,3	I5,6	I9,8	I8,8	I5,4	II,2
7I	I0,6	I6,2	I8,9	I8,4	I5,5	II,5
73	9,8	I5,I	I7,8	I7,7	I5,2	II,6
75	8,9	I3,9	I8,7	I8,8	I6,6	I3,0
77	9,I	I4,3	I7,3	I7,7	I5,9	I2,7
79	8,I	I2,9	I5,7	I6,3	I6,I	I4,0

Particular attention was given to the calculation of aberrations. Since coma is eliminated for the objective, its aberrations are significantly less.

The results of calculation of the distribution of intensities in the focal plane of the objective and paraboloid for mirrors of Ni and Au are shown on Figure 16-20 (Appendix, following §1.8).

Figure 21 shows the distribution of relative intensity along the xx and yy axes for an infinitely distant source, displaced by angle $\alpha = 28'$ along the x axis. In this case, the center of the image is shifted from the focal point by approximately $\alpha Lp/2$ in the case of the objective, and αLp in the case of a paraboloid. We can see from Figure 21 that for an objective, a sharp peak of intensity with a width at half height significantly less than the deviation of the ray from the axis of the system is produced at the center of the image. In the case of a paraboloid, the image has the form of a ring, its width being greater than the deviation of the ray from the optical axis of the system. /26

/25
/27

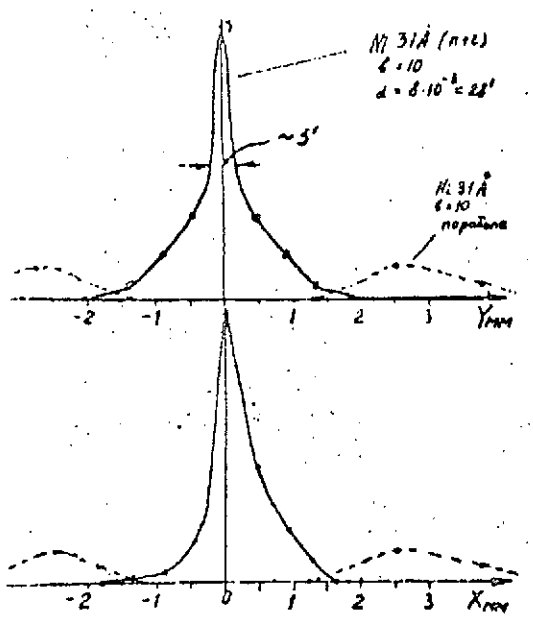

Figure 21. Distribution of Intensity in Focal Plane Along y and x Axes for an Objective (Solid Line) and a Paraboloid (Dotted Line), Based on Data of Figures 17, 20. Source Displaced Along x Axis by Angle $\alpha = 28'$

1.5.1. High-Resolution Objective

For some astrophysical problems, it is important to have the greatest possible angular or spatial resolution with comparatively low aperture ratio. Objectives with high resolution have been suggested by a number of authors (for example, see [12]). In these lenses, the image is constructed only by rays near the area of intersection of the paraboloid with the hyperboloid (similar to stopping down a diaphragm in optics). The effective area of the telescope is significantly reduced in this case, but for strong sources and, particularly, for the sun, these objectives are of great interest.

As an example of an objective designed for minimum aberrations with low effective area, let us study the objective from the work of J. D. Mangus and J. H. Underwood [7]. The parameters of this objective, in our symbols, are as follows:

Inlet aperture of paraboloid	$b = 12{,}365$ cm
Distance from inlet aperture to focal point of paraboloid	$L_p = 392.66167$ cm
"Focal" length	$F = L = 202.16167$ cm
Parameter characterizing ratio of glancing angles on paraboloid and hyperboloid	$\varepsilon \approx 1.01516$

The focus of the geometric collecting area of the objective is only 14.84 cm^2, while the effective area for a nickel coating at wavelength $\lambda = 31.36$ A $S_{ef} = 12$ cm^2.

The angular diameter of the spot (diameter in seconds of arc) from the parallel bundle of rays in the Gaussian plane, calculated according to the program presented in Chapter II (§2.1) is as follows for the following incident angles /28

$2 \cdot 10^{-3}$ rad - $\varnothing = 7''$

$4 \cdot 10^{-3}$ rad - $\varnothing = 30''$

$16 \cdot 10^{-3}$ rad - $\varnothing = 16'$

These results agree with the data of [7].

As an illustration, Figure 22 shows the distribution of intensities in the Gaussian plane with incident angle $8 \cdot 10^{-3}$ rad.

§1.6. Requirements for Manufacturing Accuracy

The development of x-ray astronomy is related to a great extent with improvement of the quality of manufacture of x-ray optics. The quality of manufacture determines both the effectiveness of the objective (i.e., the reflection factor is strongly influenced by polishing quality) and resolving properties. /29

Let us discuss manufacturing accuracy, leading to limitations in the resolution of mirror systems. In itself, a deviation from fixed dimensions, if the shape of the surface is retained, does not lead to significant distortions. Manufacturing errors can be arbitrarily divided into two groups: errors which change dimensions without changing the angle of the generatrix, and errors which involve waviness of the surface, changing

the direction of the reflected ray. The first group of errors includes: noncoaxiality of the entry and departure diameters, deviation in diameters (ΔR) and roundness -- deviations from circular shape. The limitations on this class of errors are generally rather mild.

Errors of the second group are angular and therefore directly related to the angular resolution of the objective. Their conversion to linear deviations leads to more rigid requirements as to manufacturing accuracy.

Requirements for the accuracy of manufacture of an objective necessary to achieve an angular resolution of about 1" are presented in [6]. We present below the permissible relative deviations in the manufacture of objectives with resolutions of about 1'.

Let us introduce the following symbols: δx is the linear deviation in the plane of the image, y is the ordinate (distance from relative axis) of the reflecting surface, $y' = \tan \alpha \approx \alpha$ is the inclination of the reflecting surface and $\delta y'$ is the angular error. It is then easy to produce: /30

$$\frac{\delta x}{y} = \left|\frac{\delta y}{y}\right| + \left|\frac{\delta y'}{y'}\right| \qquad (1.13)$$

The first component in the right portion of equation (1.13) represents the errors related to variations in linear dimensions. Assuming angular resolution $\delta\alpha = (2/Lp)\cdot\delta x = 3\cdot10^{-4}$ (angular minute), where L_p is the focal length of the paraboloid, formula (1.13) indicates that the maximum permissible sum of relative deviations such as roundness, ellipticity, noncoaxiality, etc., is:

$$\frac{2}{L_p}\delta y \approx 3\cdot10^{-4}$$

for a lens with Lp = 70 cm, we produce: $\delta y \approx 0.1$ mm.

The second component in equation (1.13) corresponds to relative angular errors. For an angular resolution $\delta\alpha = 3\cdot10^{-4}$, we produce:

$$3\cdot10^{-4} = \frac{2}{L_p}\delta x = \frac{2y}{L_p}\left(\frac{\delta y'}{y'}\right) \qquad (1.14)$$

If the angular error is caused by waviness of the surface such as $\delta y = h/2 \sin 2\pi(\ell/\lambda)$, where h is the height of an irregularity, λ is the period of the irregularity and ℓ is the instantaneous coordinate along the generatrix, then

$$[(\delta y)'_\ell]_{max} = \pi\frac{h}{\lambda} \qquad (1.15)$$

Substituting (1.15) into (1.14) for an objective with $(y/y')_{max} = 2\cdot F = 2\cdot65$ cm and Lp = 70 cm, with a resolution of 1', we produce:

$$\frac{h}{\lambda} \leq \frac{\delta\alpha\cdot L_p}{4\pi F} = 2{,}6\cdot10^{-5}$$

§1.7. Prospects for Applications

/31

1.7.1. Parabolic Mirrors

The use of a paraboloid for the study of soft x-ray radiation yields a number of advantages over ordinary counter telescopes, including an increase in the signal-to-noise ratio.

The focussing properties of a paraboloid allow a significant decrease in the inlet window of the counter, which is particularly important for recording radiation E < 0.3 KeV. In this area of energies, very thin organic films must be used as counter windows. The micropores in these films allow gas to leak out of the counter. It is therefore quite desirable to make the area of the inlet window as small as possible.

Furthermore, the use of a paraboloid allows other types of detectors such as secondary electron multipliers, semiconductor detectors, channel multipliers, etc. to be used.

The primary results produced up to now in x-ray mirror astronomy have been achieved using proportional flow counters as detectors. The main difficulties encountered in this method are related to the search for new thin films, capable of withstanding rather high pressures while operating for long periods

of time in a vacuum, while having good transmission properties in the 20-100 A area. Figure 23 shows the transmission factor n as a function of wavelength for 6, 1.3 and 0.42 m films of polypropylene. Based on these data and the parameters of the paraboloid yielding maximum effective area with a given focal length (F = 65 cm) (see §1.3), the overall effectiveness of a telescope was calculated. The results of calculations for coatings of Ni and Au as a function of wavelength are presented in Tables 3 and 4. Here also we present the optimal radius of the inlet aperture of the paraboloid b. It should be noted that the optimal radius, generally speaking, depends on the thickness of the film, but calculations have shown that this dependence can be ignored in practice. /33

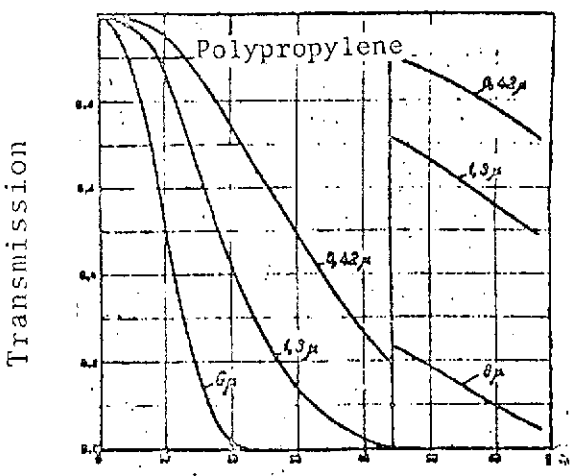

Figure 23. Transmission of Films of Polypropylene

/32

The use of a semiconductor detector, for instance silicon allied with lithium Si(Li), allows us to avoid the complex gas system of a flow counter. But difficulties arise here, related to the necessity of cooling the detector. The effectiveness of a detector of Si(Li) in the 8-50 A area is determined by the transmission of the surface layer of Si and the transmission of the filter which absorbs the ultraviolet. Figure 24 /34

TABLE 3

λ,[Å]	Optimal Radius b, cm	$S_{ef} \cdot \eta$ of film, [cm^2]	
		Thickness of Counter Window 6 μ	1,3 μ
21,6	6	~0	18
31	10	~0	11
44,4	13	45	130
67	22	22	220

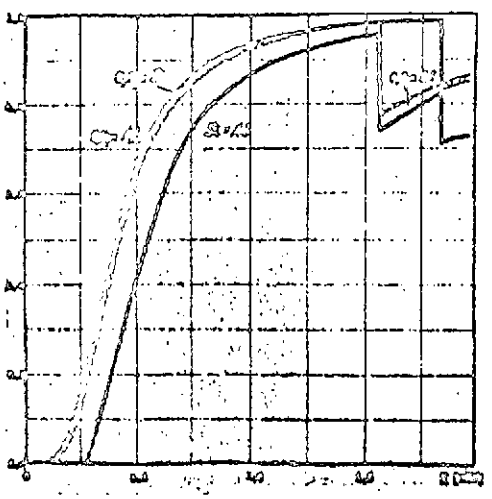

Figure 24. Transmission of Silicon and Aluminum and Summary Effectiveness of Semiconductor Detector

shows the transmission factors 0.2 μ Si and 0.2 μ Al, as well as the summary effectiveness η of a semiconductor detector, as functions of wavelength[1] [13]. Table 5 shows the maximum effectiveness of 65-centimeter nickel and gold telescopes with semiconductor detectors for a number of wavelengths. For each effectiveness, we have shown the optimal radius "b" of the entry aperture of the paraboloid.

TABLE 4

λ, [Å]	Optimal Radius b, cm	$S_{ef} \cdot \eta$ of film, [cm²]	
		Thickness of Counter Window 12 μ	0,42 μ
8,34	4	II	II,5
9,89	4	I2,5	I3,5
I2,25	5	I5	I7,7
2I,6	7	II,5	22
3I	I0	5	I9,5

Recently, considerable attention has been given to the use /35 channeltrons as x-ray radiation detectors. Channel multipliers differ favorably from counters and semiconductor detectors in their smaller dimensions, lack of an entry window (although an ultraviolet filter is apparently necessary) and higher signal level at the output.

[1]The data relate to a detector developed in the Laboratory of Physical Electronics of the Institute of Nuclear Studies (France). The authors are grateful to Dr. L. Koch for providing us with these data.

TABLE 5

λ, [Å]	Au		Ni	
	β [cm]	S_{ef} [cm^2]	β [cm]	S_{ef} [cm^2]
8	4	II,4		
I0	4	I3		
I2	5	I6,8		
22	7	I5,7	6	25
3I	I0	9	I0	20
44			I3	7,5
67			2I	0

1.7.2. Production of an X-Ray Image

The next, most difficult step consists in the production of an x-ray image of a source. The basic problem involves the development of high quality x-ray optics. The accuracies necessary for the production of an image with a resolution of about 1' can be achieved by high-precision metal working program-controlled machine tools, while resolution of one angular second lies at the limit of the capabilities of modern optical techniques.

Serious problems also arise in the development of x-ray sensors with high spatial resolution. For example, using a paraboloid and hyperboloid 1 m in length from the entry aperture to the focal point of the system as an objective, achievement of a resolution of 1' requires a detector with a resolution of about 6 [illegible]/mm. EOC's and microchanneltron discs have this level of spatial resolution at the present time.

§1.8. Appendix. Distribution of Intensities in Gaussian Plane /36

The figures presented below show the distribution of intensities in the plane of the image of the objective and of a paraboloid with F = 65 cm for a number of values of angle α of the incident beam to the optical axis. The center of the image is displaced in the positive direction of the axis by approximately $\alpha Lp/2$ for the objective and αLp for the paraboloid. The center of the frame limiting the field of vision tracks the center of the image. A rule of change of frame dimensions $(4\alpha)^{3/2}$, corresponding to the growth of aberrations, has been empirically established.

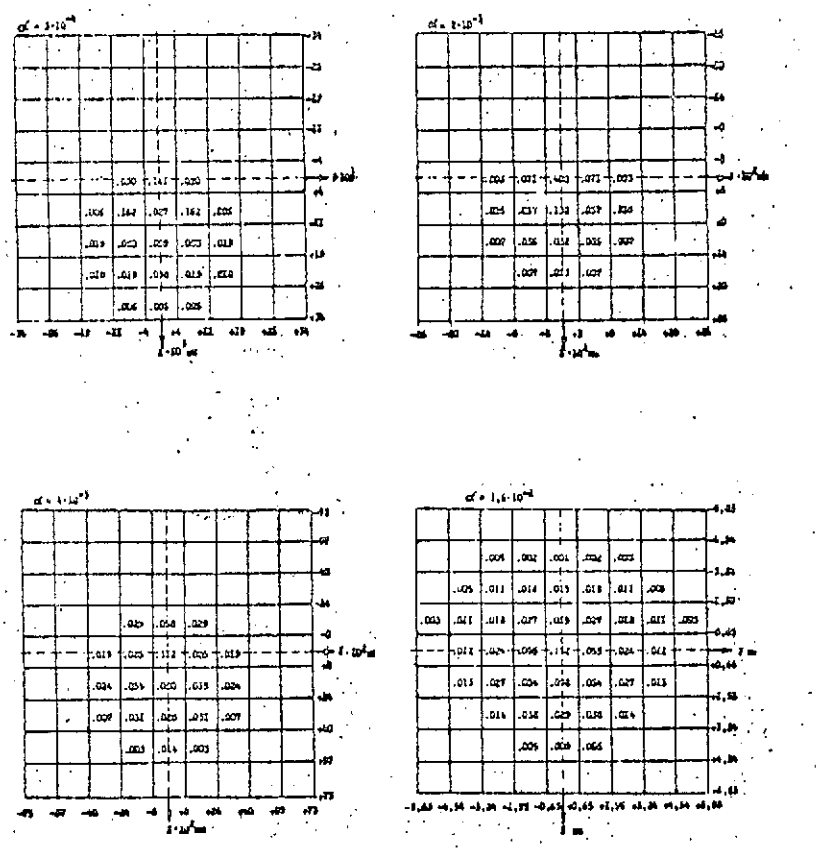

Figure 16. Distribution of Intensities in Gaussian Plane as a Function of Angle α of Parallel Bundle (44 A) to Axis of System. Objective (Parabola plus Hyperbola): Ni, b = 16 cm, Lp = 70 cm, F = 65 cm

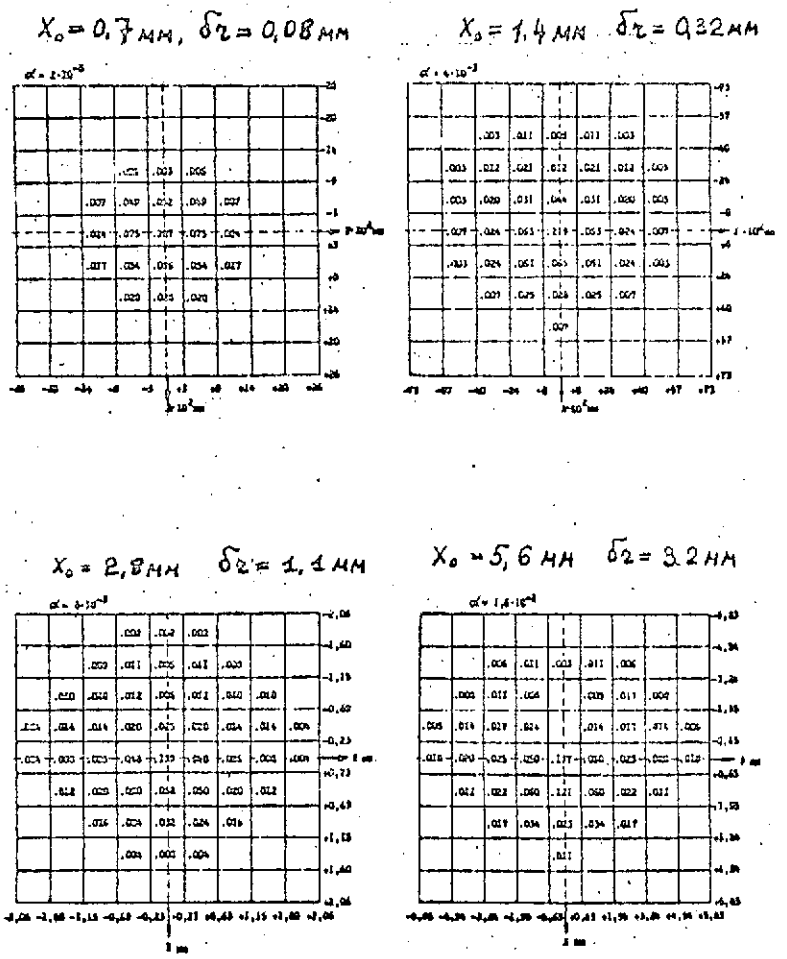

Figure 17. Distribution of Intensities in Gaussian Plane for Objective (Parabola plus Hyperbola) of Ni, b = 10 cm, Lp = 70 cm, F = 65 cm, λ = 31 A. x_0 and δr are Displacement of Center and Mean Square Radius of Distribution (See Formula in Section 2.1.5b)

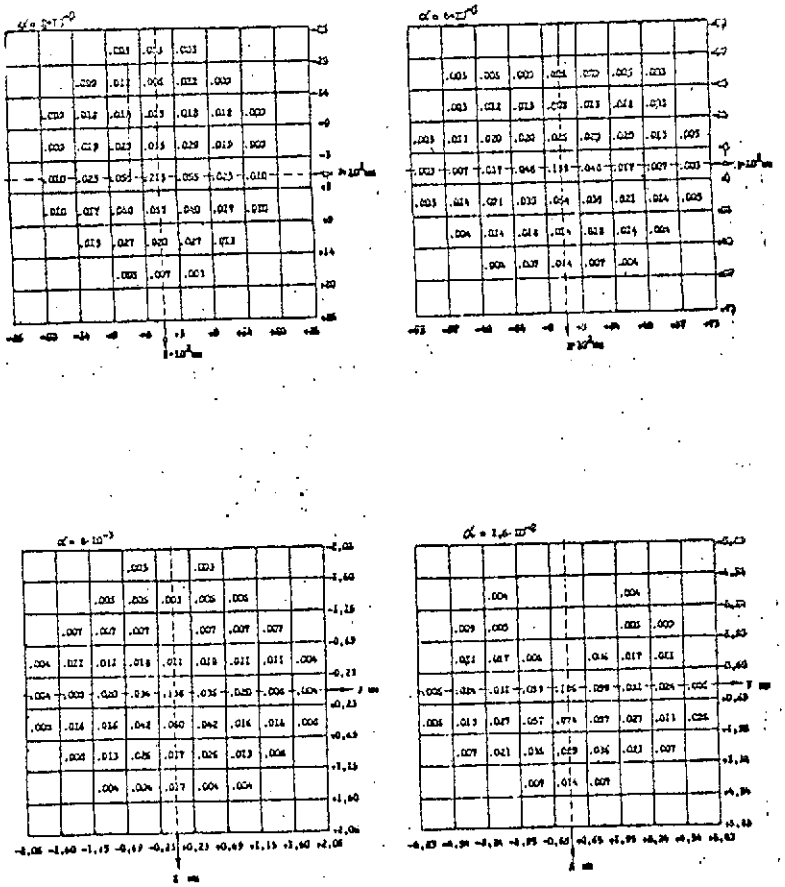

Figure 18. Distribution of Intensities in Gaussian Plane for Objective (Parabola plus Hyperbola) of Au, b = 6 cm, Lp = 70 cm, F = = 65 cm, λ = 31 A

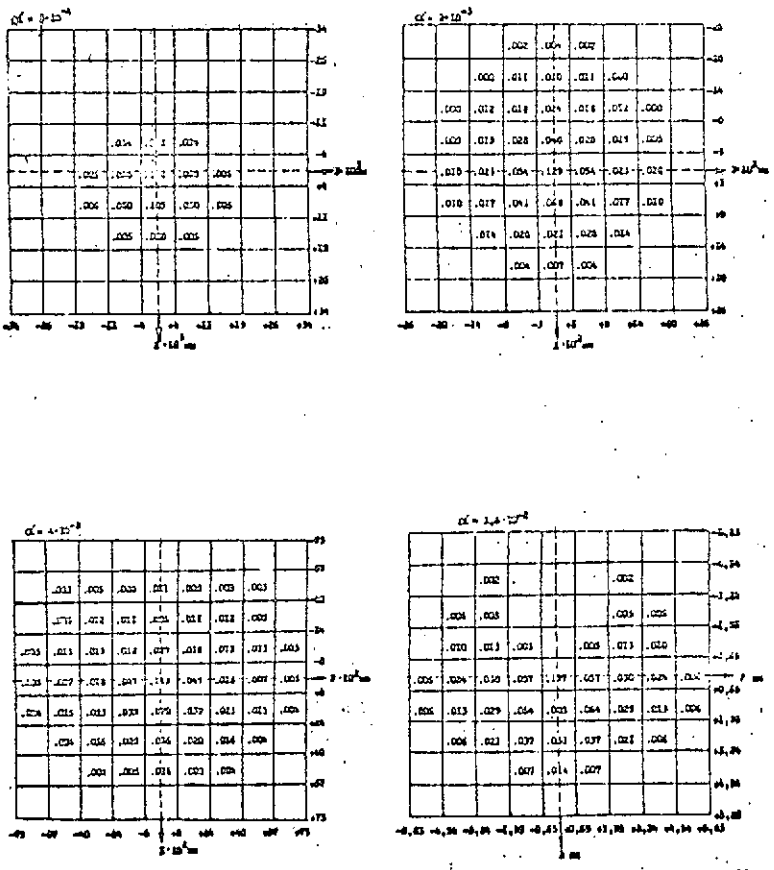

Figure 19. Distribution of Intensity in Gaussian Plane for Objective (Parabola plus Hyperbola) of Au, b = 6 cm, Lp = 70 cm, F = 65 cm, λ = 12 A

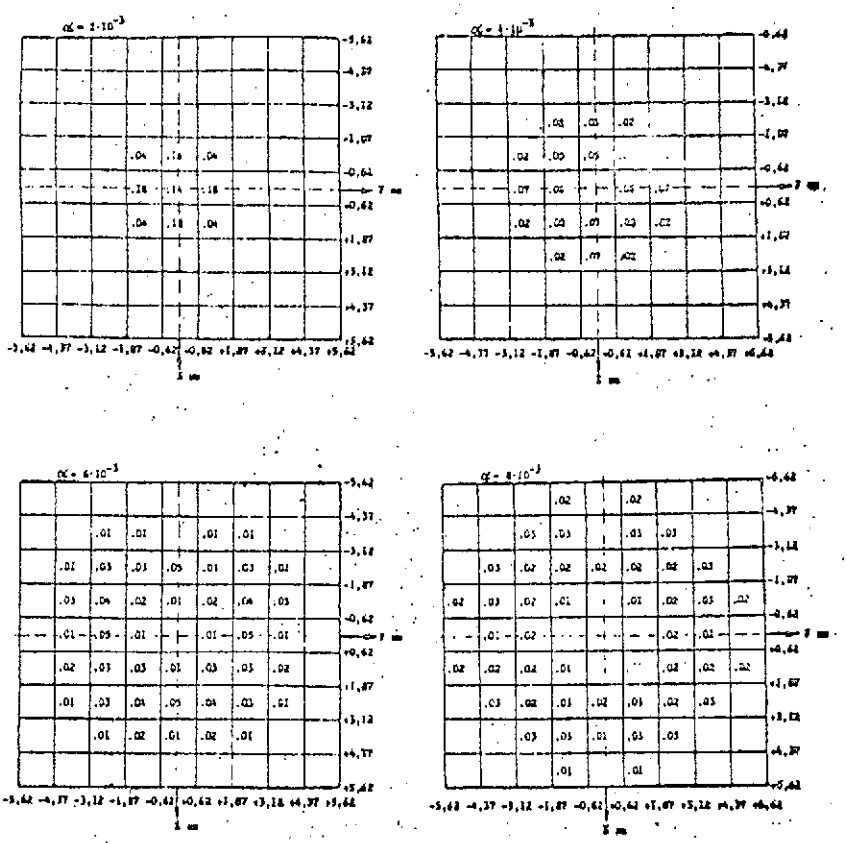

Figure 20. Distribution of Intensity in Gaussian Plane for Parabola of Ni, b = 10 cm, Lp = F = 65 cm, λ = 31 A.

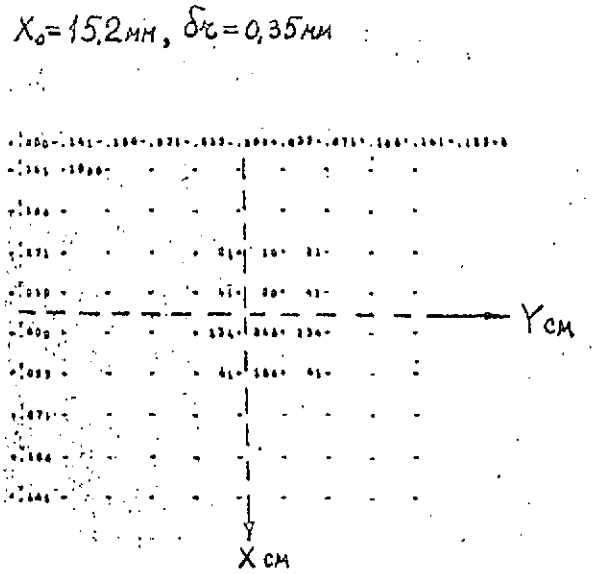

Figure 22. Distribution of Intensity in Gaussian Plane with Incident Angle $8 \cdot 10^{-3}$ rad for High Resolution Objective of Ni, b = 12.365 cm, Lp - 592.66167 cm, F = 202.16167 cm, λ = 31 A, x_0 and δr are Displacement of Center and Mean Square Radius of Distribution (See Formula in Section 2.1.5b)

Chapter II. Description of Program for Calculation of Parameters and Aberrations of Objectives and Parabolic Mirrors

/42

The "parabola plus hyperbola" problem is designed for calculation of the aberrations of an image and effective area for "parabola" or "parabola with hyperbola" telescopes in the x-ray area of the spectrum. A program to solve the problem has been written for the BESM-4 and M-220 computers.

The rules for solution of the problem are presented in §2.1; §2.2 presents the general formulas.

§2.1. Rules for Use and Order of Assembly of the Problem

The "parabola plus hyperbola" problem can be solved in two versions. In the first version, the effective area of the system S_{ef} and aberrations of the image are calculated as functions of the incident angle α of the parallel bundle to the axis of the system. Due to the symmetry of the system, quadrants I and IV of the entry aperture are used:

In the second version, the table of values of S_{ef} is calculated (where $\alpha = 0$) as a function of the values of the entry aperture radius (b) and focal length of the paraboloid (Lp) (see Figure 15). The top row of the table is the effective area of a "pure" parabola. /43

The basic program is recorded on magnetic tape in the general program for calculation of atomic characteristics (FIAN Preprint No. 87, L. A. Vaynshteyn, V. P. Shevel'ko, 1970), zones 7 and 12. The problem allows any number of versions to be calculated. The sign of completion of work is the instruction "enter."

2.1.1. Sequence of Assembly of the Problem

Version Number 1

1. Input punch card (read zones No. 7 and 12 of magnetic tape).

2. Punch card -- full circle version (see 2.1.5a) plus possible supplementary punch cards and zero check sum (ΣK).
3. Various versions with ΣK each.

It should be noted that the action of the punch cards input in No. 2 extends to all versions assembled in No. 3. The action of the punch cards input in No. 3 extends only to individual versions.

Version Number 2 /44

In place of the punch card of the full circle version in No. 2, punch cards No. I and IV ("Tables") (see Section 2.1.5e) are used.

2.1.2. Distribution of Memory (Core)

Locations 50-77 -- constants; assigned in 10th system.

Locations 100-610, 2400-2525 -- program.

All linear dimensions in the program are fixed in cm, areas -- in cm^2, angles -- in radians.

Constants (Standard Version)

Location Number	Print	Symbol	Numerical Value	Explanation (See Fig. 15)
50	BO	b	12	Radius of engry aperture
51	LO	l	65	Distance from entry aperture to plane in question
52	PO	p	Calculated	Parameter of parabola
53	AO	a	"	Parameters of hyperbola
54	ZR	z_r	"	Parameters of hyperbola
55	C2	c^2	"	Parameters of hyperbola
56	RM	r_m	0.5	Radius of circle studied in plane L
57	LI	lp	70	Focal length of parabola
60	ZI	z_1	Calculated	Length of parabola
61	NF	N_ϕ	3	Number of points of subdivision of angle ϕ /45
62	NP	N_p	41	Number of points of subdivision of radius p

Location Number	Print	Symbol	Numerical Value	Explanation (See Fig. 15)
63	DA	$\Delta\alpha$	$2\cdot10^{-3}$	Step of α
64	AM	α_m	$2\cdot10^{-2}$	Maximum angle α
65	FO	F^m	65	Focus of system
66	ShO	δ	$2.7\cdot10^{-2}$	Parameters determining
67	ShchO	β	$7.1\cdot10^{-3}$	reflection factor (for Ni 44A) (see §1.2)
70	PI	p_1	8	Entry diaphragm
71	EO	ε	1	Ratio of angle of reflection at entry of parabola to angle of reflection at exit of parabola
72	0	0	0	
73	Not printed	ε_1	0.75	Portion of length of parabola used
74	"	b_0	10	Initial values of
75	"	Δb	2	b_0, Lp^0) and steps
76	"	Lp^0	65	
77	"	ΔLp	2	(Δb, ΔLp) for table in mode of Version No. 2

2.1.3. Calling of Reflection Factors /46

κ	16	$\kappa + 1$	550	601

Before calling the reflection factor κ, $\vec{n}\vec{N}$ -- location 41 must be sent. Result κ is placed in location 4.

2.1.4. Interpretation of printout.

Version Number 1

Following the parameters, the distribution of intensity in the plane of the image is printed with a fixed value of angle α. The distribution near the center of the spot is printed. The dimensions of an area which is printed: $r'_m = 2^8 \cdot \alpha^{3/2}$ -- this rule corresponds approximately to the increase in the aberrations. S^n_{ef} is the full effective area for dimension r_m. In the left top corner, the ratio S_{ef}/S^n_{ef} is printed, where S_{ef} is the effective area for the size of a printed area (r'_m).

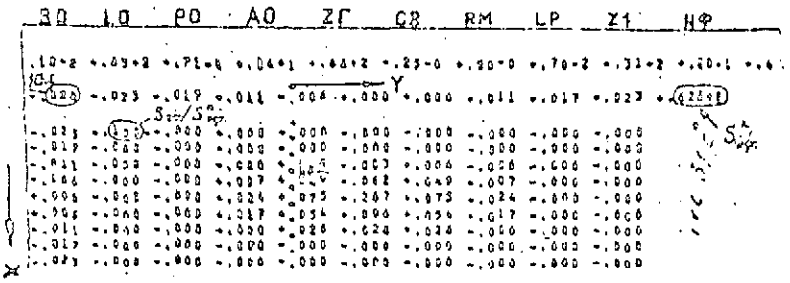

Example 1. Interpretation of Printout of Aberration

When $L_p < F$ is fixed, the aberrations and S_{ef} for a system consisting of one parabola will be printed. /47

Version Number 2

(Table S_{ef})

After printing the parameters, Table S_{ef} is printed as a function of b and Lp (total of 6 columns b and 8 rows Lp):

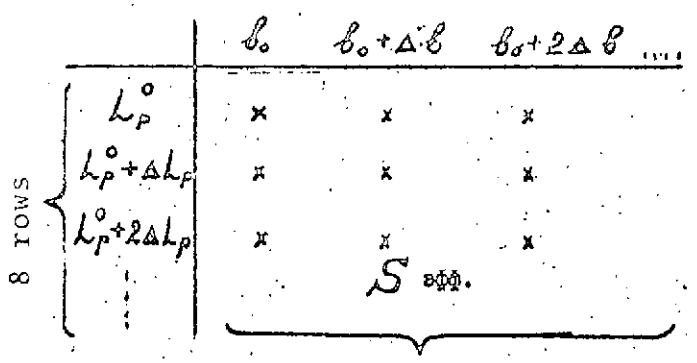

Here, the row with Lp^0 gives the value of S_{ef} for a system consisting of one parabola.

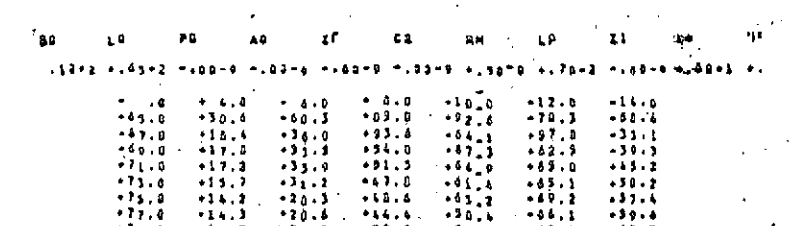

Example 2. Printing of Table of Effective Area

2.1.5. Additional Versions /48

Supplementary punch cards with instruction are inserted before OKΣ of the problem or an individual version (for more detail, see section 2.1.1, Order of Assembly of Problem).

a. Full Circle Version (for No. 1)

Used in Version No. 1

Text of Punch Card:

		I3I		KA
0I.	003I.	0077.	0	
		77		KA
+0I.	46I.	0.	0.	
		05I6		KA
0I.	003I.	0077.	0.	

b. Automatic Selection of Frame (for No. 1)

In calculating aberrations of objectives with parameters differing significantly from the standard parameters, it is difficult to guess the size of the frame in advance. Therefore, punch cards 1A-5A for automatic frame selection are inserted. In this case:

a) Only those rays which intersect the plane of the image at a distance less than r_m from the main optical axis of the system are considered.

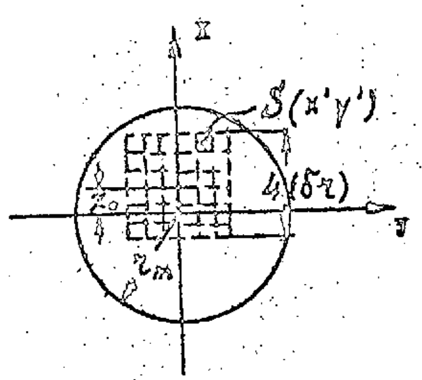

b) The following quantities are calculated:

$$X_0 = \frac{\int x' \cdot S(x'y')\, dx'dy'}{\int S(x'y')\, dx'dy'}$$

and $(\delta r) = \sqrt{(\delta x)^2 + (\delta y)^2}$,

where $(\delta y)^2_{y_0=0} = \frac{\int (y')^2 S(x'y')\,dx'dy'}{\int S(x'y')\,dx'dy'}$,

$(\delta x)^2 = \langle x^2 \rangle - x_0^2$,

but $\langle x^2 \rangle = \frac{\int (x')^2 S(x'y')\,dx'dy'}{\int S(x'y')\,dx'dy'}$

(All integrals are taken with respect to a circle of radius r_m in the plane of the image).

c) The center of the frame coincides to x_0; the length of a side of the frame is $4 \cdot (\delta r)$.

Interpretation of the printout is illustrated in Example 1 in section 2.1.4.

The text of the punch cards for automatic frame selection is as follows:


```
                2527          IIA                    IA
0 2527 005 0046 00I0 000I }
0 2530 00I 0656 000I 0656 } <x>
0 253I 005 0006 00I0 000I }
0 2532 00I 0655 000I 0655 } <x²>
0 2533 005 0007 00I0 000I }
0 2534 00I 0654 000I 0654 } <y²>
0 2535 002 0046 0652 0046   x''-x₀
0 2536 005 0046 0046 000I }
0 2537 00I 000I 0007 000I } ρ'=√((x''-x₀)²+y²)
0 2540 044 000I 0000 00II }
0 254I 002 00II 0056 0000   ρ-rm

0 2542 076 0040 0I30 065I ← α ← Print   2A
0 2543 0I6 0000 0350 0000 Out ← 350
```

c. Printing of Parameters with 9 Characters (for No. 1) /52

The contents of locations 50-76 are printed with 9 characters.

Text of Punch Cards:

```
     222          KA
16. 0223 750I 76I0
52. 0050 0027 0076
```

d. Printing without Shifting of Center of Image in Frame (No. 1)

Used in Version No. 1. Here, the plane studied is in the center of the image.

Text of Punch Cards:

```
     332.         KA
I6. 0333 2530 2534
     2530         KA
0I. 00I6 0002 0047   y''
05. 0040 0065 000I } x''-aF
02. 0046 000I 0046 }
 0   0   0   0
```

e. Printing in 16 Positions (for No. 1)

Used in Version No. 1 for production of more detailed picture of aberrations.

```
     44I          KA
I00 0656   0 066I
     430          KA
50I 0700 0656 0700
     352          KA
 0I 0656 00I0 0656
     433          KA
 06 0075 0056 000I
     522          KA
306 0I03 000I 000I
     542          KA
 06 0030 2000 0I74
```

/53

f. Printing of "Table" (Punch Cards I-IV for No. 2)

		270I			KA	I
I06 →		02	74	75	50	$\delta_0 - \Delta\delta \to \delta$
27I6 →		0I	50	75	50	$\delta + \Delta\delta$
		72	0	II0	0	
	6	52	II	0	II0	
		02	76	77	57	$L_p - \Delta L \to L$
	I	00	50	0	3000	$\delta \to$ Table
27I5 →		0I	57	77	57	$L_p + \Delta L \to L_p$
27I0	4	52	0	0	27I3	
		I6	27I2	2743	2745	→ to Read Program
		56	50	230	25	→ to Calculate S
				0		[Illegible]
	I	06	0I0I	0677	300I	2(S/2) → Table II
	I	40	0II0	2707	000I	→ [New?] Lp
		I2	0II0	2702	0	
		0	0076	0	2770	$L_p \to$ Table
2720	5	0I	2770	0077	277I	
	I	I2	0006	2720	000I	
		I6	2723	750I	76I0	
		52	2725	0I62	273I	
		I6	00I2	0I00	0	
		0	0002	2767	00I0	
		0	000I	000I	0	
		02	0	00II	00I0	
		03	00I3	3II0	0070	III
			0222		KA	
		56	0	0III	0	[Area?] Print Parameters
			0442		KA	
		56	0	0I37	0	b/Print Field of Vision
			0I4I		KA	
		56	0	27I3	0	
			27II		KA	
		I6	27I2	2743	2745	
			2736		KA	
I07 →		I6	2737	750I	76I0	Print Parameters
		52	0456	0I62	0467	

/54

```
        I6 274I 7500 76I0                    IV
        I5 0III 0001 2550
         0   0   0        ← PU Calculate
27II →  I6 2744 7500 76I0
        II 0III 0001 2550
           0I05          KA
        02 0076 7757 0076   Lp−ε → Lp
        I6 270I 2736 2742   Print Parameters
           0III          KA
         0   0   0  0040
           0051          KA
Number → 0I  200   0   0    Nφ = 2

           0246          KA                    V
        55   0 2750   0
        05 0077 000I 000I  } a = Lp − F/2 · cos γ
        05 000I 0005 0053  }
           2750          KA
        55 0337 7735 0337
        05 0055 0073 0060   z1 for Parabola
        55 2516 0276 0325
           0I23          KA
        05 0077 0050 0032   g = δ/2
```

/55

g. Increase Points of "b" (for No. 2)

Used in Version Number 2. The number of columns "b" is increased to 16.

Text of Punch Card:

```
   2716          KA
I2 0220 2702  0
   2730          KA
03 00I3 3220 0170
```

§2.2. Formulas for Calculation of Path of Rays and Parameters of Paraboloid and Hyperboloid

/56

With existing manufacturing accuracies, the quality of the image is clearly worse than the limits imposed by diffraction theory. Therefore, the entire calculation is performed within the framework of geometric optics.

2.2.1. Formulas for Calculation of Parameters of Objective

The paraboloid parameter "p" and distance from its point to the entry aperture are determined from the formulas:

$$p = -L_p \pm \sqrt{L_p^2 + \beta^2} \tag{2.1}$$

$$z_p = \frac{\beta^2}{2 \cdot p} \tag{2.2}$$

where Lp is the "focal" length of the paraboloid.

The confocal condition of the parabola and hyperbola:

$$\frac{L_p - F}{2} = \sqrt{a^2 + c^2} \tag{2.3}$$

$$z_c = F + \frac{L_p - F}{2} = \frac{F + L_p}{2} \tag{2.4}$$

where F is the focal length of the system, the remaining symbols are the same as in §1.5.

/57

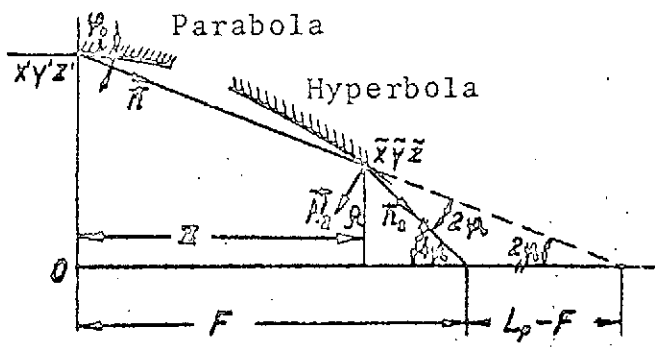

Figure 25. Condition of Equality of Glancing Angles

Constants "a" and "c" are found from the condition of equality of the glancing angles on the parabola and hyperbola for the extreme ray (see Figure 25): /58

Introducing the symbols

$$a = \cos\gamma\sqrt{a^2 + c^2} \tag{2.5}$$

$$c = \sin\gamma\sqrt{a^2 + c^2} \tag{2.6}$$

$$u = \sin^2\gamma \tag{2.7}$$

and using (2.3), we produce

$$a = \frac{L_p - F}{2}\cdot\cos\gamma \tag{2.8}$$

$$c = \frac{L_p - F}{2}\cdot\sin\gamma \tag{2.9}$$

Angle γ can be expressed through glancing angle ϕ_0 of the extreme ray. Using the equality of angles (Figure 25)!

$$\left.\begin{aligned} \rho &= (L_p - F)\sin 4\varphi_0 \\ x &= F - (L_p - F)\cos 4\varphi_0 \end{aligned}\right\}$$ Substituted in equation for hyperbola

considering (2.7-2.9), we produce an equation for "u":

$$\frac{u^2}{4} + u(1 + \cos 4\varphi_0) - \sin^2 4\varphi_0 = 0$$

$$u \simeq 8\varphi_0^2$$

$$u = \sin^2\gamma_0 \simeq \gamma_0^2 = 8\varphi_0^2 \qquad \gamma_0 = 2\sqrt{2}\,\varphi_0$$

Since for the extreme ray $\varphi_0 = \frac{\delta}{2L_p}$, then

$$\gamma_0 = \frac{\sqrt{2}\,\delta}{L_p} \tag{2.10}$$

In the program $\gamma = \gamma_0 \cdot \varepsilon$, where γ_0 is defined from (2.10), ε is varied within limits of $0.8 \leq \varepsilon \leq 1.2$. /59

After finding "a" and "c", we determine the length of the parabola z_1:

$$\left.\begin{cases}\dfrac{(z-z_r)^2}{a^2}-\dfrac{\rho^2}{c^2}=1\\ \rho^2=2p(z_p-z)\end{cases}\right\}\underbrace{c_1}_{a_1}z_1^2-2z_1\underbrace{(c_1z_r-c_2)}_{a_2}+\underbrace{c_1z_r^2-2c_2z_p-1}_{a_3}=0$$

$$c_1=1/a^2;\quad c_2=p/c^2;\quad c_2\gg c_1$$

$$z_1=\frac{a_2-\sqrt{a_2^2-a_1a_3}}{a_1} \tag{2.11}$$

2.2.2. Coordinates of Point of Intersection and Direction of Ray Reflected from Parabola with Hyperbola (See Figure 25)

The equation for a ray reflected from a parabola at point x', y', z' in the direction of vector $\vec{n}\{n_x, n_y, n_z\}$:

$$\begin{cases}x=x'+\dfrac{n_x}{n_z}(z-z')\\ y=y'+\dfrac{n_y}{n_z}(z-z')\end{cases}\qquad \frac{n_x}{n_z}=\alpha;\ \frac{n_y}{n_z}=\beta$$

The coordinates of intersection of the ray with the hyperbola (point $\tilde{x}$, $\tilde{y}$, $\tilde{z}$) can be found by substituting:

$$\tilde{x}=x'+\alpha(\tilde{z}-z')=x'+\alpha f \qquad /60$$

$$\tilde{y}=y'+\beta(\tilde{z}-z')=y'+\beta f$$

where f = z - z', into the equation for the hyperbola. For f we produce

$$f=\tilde{z}-z=\frac{-a_2+\sqrt{a_2^2-a_1a_3}}{a_1}$$

where

$$a_1 = \frac{1}{a^2} - \frac{\alpha^2 + \beta^2}{c^2}$$

$$a_2 = \frac{x' - x_c}{a^2} - \frac{x'\alpha + y'\beta}{c^2}$$

$$a_3 = -\frac{x'^2 + y'^2}{c^2} + \frac{(x' - x_c)^2}{a^2} - 1$$

The normal $\vec{N}_2$ and point $\tilde{x}$, $\tilde{y}$, $\tilde{z}$:

$$\vec{N}_2 \left\{ \frac{m_1}{N}; \frac{m_2}{N}; -\frac{1}{N} \right\}$$

where $m_1 = \frac{a^2 \tilde{x}}{c^2(\tilde{z} - z_c)}$; $m_2 = m_1 \cdot \frac{\tilde{y}}{\tilde{x}}$; $N = \sqrt{m_1^2 + m_2^2 + 1}$

The unit vector of a ray reflected from the hyperbola:

$$\vec{n}_2 = \vec{n} - 2(\vec{n} \cdot \vec{N}_2)\vec{N}_2 \qquad \text{(Theorem of Reflection)}$$

Let us represent $\vec{n} \cdot \vec{N} = g$. Then the projections of vector $\vec{n}_2$ on the axes of the coordinates are:

$$n_{2x} = n_x - 2g N_{2x}$$

$$n_{2y} = n_y - 2g N_{2y}$$

$$n_{2z} = n_z - 2g N_{2z} = n_z + \frac{2g}{N}$$

REFERENCES

1. Yentis, D. J., R. Novick and P. Vanden Bout, Aph. J., 177, No. 2, Part 1, pp. 365-373; 375-396, 1972. /61
2. Yentis, D. J., J. R. P. Angel, D. Mitchell, R. Novick and Vanden Bout, P. 1971, "New Techniques in Space Astronomy, IAU Symp. 41, pp. 145-158.
3. Beygman, I. L., L. A. Vaynshteyn, Yu. P. Voynov, D. A. Gaganov, V. D. Ivanov, N. I. Komyak, S. L. Mandel'shtam, I. P. Tindo, N. A. Shatskiy, A. I. Shurygin, "X-Ray Submillimeter and Radiotelescopes," (Trudy FIAN, Vol. 77), Nauka Press, Moscow, 1973.
4. Wolter, H., Ann. Phys. 10, 94, 1952.
5. Wolter, H., Ann. Phys. 10, 286, 1952.
6. Giacconi, R., W. P. Reidy, G. S. Vaina, L. P. Van Speybroeck and T. F. Zehnpfennig, Space Science Reviews, Vol. 9, No. 1, 3(1969).
7. Mangus, J. D., J. H. Underwood, Appl. Opt., Vol. 8, No. 1, 1969, pp. 95-102.
8. Vaina, G. S., W. P. Reidy, T. Zehnpfennig, L. Van Speybroeck, R. Giacconi, Science, 161, pp 675-567, 1968.
9. Van Speybroeck, L. P., R. C. Chase, T. F. Zehnpfennig, Appl. Opt., 10, No. 4, p. 945, 1971.
10. Yershov, O. A., I. A. Brytov, A. P. Lukirskiy, Opt. i Spektr. 22, pp 127, 1967.
11. Likirskiy, A. P., Ye. P. Savinov, O. A. Yershov, Yu. F. Shepelev, Opt. i Spektr., 16, p. 310, 1964.
12. Van Speybroeck, L. P., A. V. Krieger, G. S. Vaina, Nature, 277, p. 818, 1970.
13. Koch, L., Personal Communication, 1973.